

# Transitions in heat transport by turbulent convection for $Pr = 0.8$ and $10^{11} \leq Ra \leq 10^{15}$

Guenter Ahlers<sup>1</sup>, Denis Funfschilling<sup>2</sup> and Eberhard Bodenschatz<sup>3,4,5</sup>

<sup>1</sup>Department of Physics, University of California, Santa Barbara, CA 93106, USA

<sup>2</sup>LSGC CNRS - GROUPE ENSIC, BP 451, 54001 Nancy Cedex, France

<sup>3</sup>Max Planck Institute for Dynamics and Self Organization, D-37073 Göttingen, Germany

<sup>4</sup>Institute for Nonlinear Dynamics, University of Göttingen, D-37073 Göttingen, Germany

<sup>5</sup>Laboratory of Atomic and Solid-State Physics and Sibley School of Mechanical and Aerospace Engineering, Cornell University, Ithaca, New York 14853

## Abstract.

We describe a pressure vessel for conducting experiments in helium (He), air, nitrogen ( $N_2$ ), or sulfur hexafluoride ( $SF_6$ ) under pressures of up to 19 bars, and facilities for the study of Rayleigh-Bénard convection inside this pressure vessel. The convection cells, known as the High Pressure Convection Facilities of HPCF, can have interior heights up to  $L = 2.3$  m and diameters up to  $D = 1.2$  m.

Measurements of the Nusselt number  $Nu$  for Rayleigh numbers  $Ra$  up to  $Ra^* = 4 \times 10^{13}$  and a Prandtl number  $Pr \simeq 0.8$  gave  $Nu \propto Ra^{\gamma_{eff}}$  with  $\gamma_{eff} \simeq 0.308$ . At  $Ra^*$  there was a sharp transition to a new regime. The Nusselt number was continuous at  $Ra^*$ , but the exponent characterizing its dependence on  $Ra$  changed suddenly to  $\gamma_{eff} = 0.25$ . Near  $Ra = Ra^{**} \simeq 3 \times 10^{14}$ , there was a further change in the  $Ra$ -dependence of  $Nu$ . A new state with  $\gamma_{eff} \simeq 0.17$  evolved and there was bistability of the  $\gamma_{eff} = 0.25$  and the  $\gamma_{eff} = 0.17$  branches.

**Contents**

**1 Introduction 2**

**2 Pure gases under pressure and large values of  $Ra$  6**

**3 The apparatus 7**

3.1 The pressure vessel . . . . . 7

3.2 The High-Pressure Convection Facility (HPCF) . . . . . 7

3.2.1 The HPCF structure. . . . . 7

3.2.2 Heating and cooling of the plates. . . . . 12

3.2.3 Thermometry. . . . . 13

**4 Top- and bottom-plate correction 13**

**5 Results 15**

**6 Summary and discussion 17**

**1. Introduction**

Turbulent convection in a fluid heated from below (Rayleigh-Bénard convection or RBC) has been a fascinating topic of research for a long time for theorists as well as for experimentalists.[1, 2, 3] The persistent interest has its origin in two places. On the one hand, RBC is of importance in numerous astrophysical, geophysical, and industrial processes. It occurs in Earth’s outer core[4, 5], atmosphere[6, 7], and oceans[8, 9], and is found in the outer layer of the sun[10] and in giant planets[11]. However, these complex processes, which often involve magneto-hydrodynamics, do not lend themselves readily to quantitative laboratory or numerical study with well controlled and relevant boundary conditions and appropriate control-parameter values. Thus, physicists often have focused on a particular idealized part of the complex problem where quantitative work by experiment or direct numerical simulation (DNS) becomes possible. One such idealization is convection in a right-circular cylinder of aspect ratio  $\Gamma \equiv D/L$  ( $D$  is the diameter and  $L$  the height) with a vertical axis, heated uniformly from below and cooled thusly from above. This is the system on which we shall focus in this paper.

The other source of fascination is that turbulent convection in idealized geometries is rich in important physical phenomena. From the fluid mechanics viewpoint, it is of interest for instance because it is influenced strongly over wide parameter ranges by the physics of boundary layers (BLs).[1] In part the present work may be regarded as a search for the breakdown of this boundary-layer domination[12, 13] which might be expected when the applied temperature difference  $\Delta T$  becomes sufficiently large (see, *e.g.*, [14]) Equally interesting is that the system provides a tractable example of interactions between large and small scales which are broadly important in fluid-flow problems. For

cylinders with  $\Gamma = \mathcal{O}(1)$  the large scale usually consists of a single convection roll (the large-scale circulation or LSC), with upflow and downflow near the wall but separated azimuthally by  $\pi$ . This LSC exists in the presence of vigorous small-scale fluctuations that can be treated as a noise source that acts upon the LSC.[15, 16, 17, 18]

In the present paper we focus on the heat transport as expressed by the Nusselt number

$$Nu = \frac{QL}{A\Delta T\lambda}. \quad (1)$$

Here  $Q$  is the applied heat current,  $A$  the sample cross-sectional area, and  $\lambda$  the thermal conductivity. In this system there are only two parameters which, in addition to  $\Gamma$ , are expected to determine  $Nu$ . They are the dimensionless temperature difference as expressed by the Rayleigh number

$$Ra = \frac{\alpha g \Delta T L^3}{\kappa \nu} \quad (2)$$

and the ratio of viscous to thermal dissipation as given by the Prandtl number

$$Pr = \nu/\kappa. \quad (3)$$

Here  $\alpha$  is the thermal expansion coefficient,  $g$  the gravitational acceleration,  $\kappa$  the thermal diffusivity, and  $\nu$  the kinematic viscosity.

Up to  $Ra \simeq 10^{12}$  quantitative measurements of  $Nu(Ra, Pr)$  exist over a range of  $Pr$ . [1] For  $Pr \gtrsim 3$  they show that  $Nu$  is at most weakly dependent on  $Pr$  and that it can be represented quite well by an effective power law

$$Nu = Nu_0 Ra^{\gamma_{eff}} \quad (4)$$

with  $\gamma_{eff}$  changing from about 0.28 near  $Ra = 10^8$  to about 0.31 near  $Ra = 10^{10}$  or larger. In this parameter range the heat transport is determined primarily by thermal boundary layers, one above the bottom and the other below the top plate.

The LSC passes below the top and above the bottom plate, let us say with a maximum speed  $U$ ; but directly at the plates the velocity has to vanish. This boundary condition leads to a vertical gradient of the horizontal velocity component, *i.e.* the LSC creates a sheared *viscous* BL. When  $Ra$  is not too large, the LSC Reynolds number  $Re = UL/\nu$  is also of modest size and the viscous BLs remain laminar, even though they are subject to significant velocity and temperature fluctuations because of their proximity to the turbulent sample interior and because of the emission of plumes of relatively hot or cold fluid from the thermal BLs which, depending on  $Pr$ , are imbedded in or extend beyond the viscous BLs. However, it is expected that there is a typical value  $Ra^*$  in the neighborhood of which  $Re$  reaches a value  $Re^*$  which is sufficiently large to cause a shear-induced instability of the viscous BL to a turbulent state. It is expected that this point will be reached when the *shear* Reynolds number  $Re_s = Re\lambda_\nu/L$ , based on the BL thicknesses  $\lambda_\nu$ , reaches a critical value which is believed to be somewhere near  $Re_s^* \simeq 420$  [19]. Although the value of  $Ra^*$  is quite uncertain, estimates suggest [20] that  $Ra^* \propto Pr^{0.7}$  with  $Ra^*(Pr = 1) \simeq 3 \times 10^{14}$ .

The properties of the state that is expected to exist for  $Ra > Ra^*$  have been analyzed theoretically long ago by Kraichnan.[13]. In the absence of any boundary layers he predicted that  $Nu \propto Ra^{1/2}$ . However, in the physical system with rigid top and bottom plates the fluid flow is still constrained to vanish at the walls. Thus, even though there is no laminar BL for  $Ra > Ra^*$ , there still remains a “viscous sublayer” which, in the Kraichnan theory, modifies the simple power law with  $\gamma = 1/2$  and yields  $Nu \propto Ra^{1/2}/[\log Ra]^{3/2}$ . In our range of  $Ra$  this leads approximately to  $Nu \propto Ra^{\gamma_{eff}}$  with  $\gamma_{eff} \simeq 0.4$ .

The predicted large- $Ra$  state is of interest for two reasons. On the one hand, it involves new physics that experimentalists and theorists are anxious to explore. On the other, this state is expected to be the asymptotic state that will prevail as  $Ra \rightarrow \infty$ . Any extrapolation of laboratory measurements to values of  $Ra$  relevant to many astrophysical and geophysical phenomena, which often involve values of  $Ra$  well above  $10^{20}$  (see, for instance, [21]), require an understanding of this state. Thus a significant experimental effort has been invested in reaching values of  $Ra$  much larger than  $Ra^*$ . [1]

Looking at Eq. 2 one sees that large  $Ra$  can be reached in two ways. On the one hand one can choose a fluid for which the property combination  $\alpha/\kappa\nu$  has unusually large values. It was realized long ago that gaseous and liquid helium at cryogenic temperatures offer exceptional opportunities for the achievement of a wide range as well as of very large values of  $Ra$ . [22, 23, 24] This approach was pursued by a group in Chicago [25] and a bit later by a group in Grenoble [26, 27, 28], who used fluid helium near its critical point in the vicinity of 5 K and 2 bars and reached  $Ra$  values as large as  $10^{15}$ . On the other hand, one could build a sample cell of exceptionally large height  $L$ . The strong dependence of  $Ra$  on  $L$  led to the proposal of a convection cell, using fluid helium, with  $L = 10$  m and  $D = 5$  m, first at the super-conducting super-collider before its demise, and then at Brookhaven National Laboratories, where already existing large helium liquefaction facilities could be used. [29] Such a large facility in principle should be able to achieve values of  $Ra$  as large as  $10^{19}$  or perhaps even  $10^{20}$ , which are approaching values relevant in astrophysics and geophysics; but it has yet to be built. However, a combination of a more modest but still large  $L = 1$  m and cryogenic helium enabled a group in Oregon [30] to attain theretofore unprecedented values of  $Ra$  near  $10^{17}$ .

We do not wish to review once again all of these pioneering measurements; a bit more detail can be found in a previous publication [14]. Here we only mention that the Grenoble group reported measurements that indicated the existence of a transition in  $Nu(Ra)$  at  $Ra \simeq 10^{11}$  to a state with  $\gamma_{eff} \simeq 0.4$  which they interpreted [27] as the transition to the asymptotic, or Kraichnan, state even though it occurred at a rather low value of  $Ra$ . On the other hand, the Oregon group did not find any transition all the way up to  $Ra \simeq 10^{17}$  and could describe their results over their entire range of  $Ra$  by Eq. 4 with  $\gamma_{eff} \simeq 0.32$  [31]. Although it is not known why these two experimental results differ from each other, it was noted that for both of them the Prandtl number increased as  $Ra$  became large, and that over most of the  $Ra$  range  $Pr$  was larger for the

Grenoble data than it was for the Oregon data (see, for instance, Fig. 2 of [14]).

The as yet unexplained difference between the Grenoble and the Oregon measurements on this important issue provided some of the motivation for the present work. Our experiment was designed to yield data for  $Nu(Ra)$  over a wide range of  $Ra \lesssim 10^{15}$  and for a nearly constant  $Pr \simeq 0.8$ . Rather than repeating the previous measurements, we wanted to use quite different experimental techniques and fluids. Thus the experiment was conducted with classical gases at near-ambient temperatures and at elevated pressures. Using a sample that was about 2 meters high and various gases at pressures up to 19 bars we were able to cover the range  $10^9 \lesssim Ra \lesssim 10^{15}$  (the measurements over the range  $10^9 \lesssim Ra \lesssim 10^{11}$  were done with helium; they were reported before [32] and will not be discussed in the current paper). One sees that our largest  $Ra$  exceeded estimates of  $Ra^*$  by an order of magnitude.

As reported briefly before [14], we did not find a transition in  $Nu(Ra)$  near  $Ra = 10^{11}$  where the Grenoble data revealed a change. Up to  $Ra \simeq 4 \times 10^{13}$  our data are reasonably consistent with the Oregon data, although our Nusselt values are slightly lower and our effective exponent  $\gamma_{eff} = 0.308$  is also a bit lower than their  $\gamma_{eff} = 0.32$  [31]. However, near  $Ra = Ra^* = 4 \times 10^{13}$  our measurements show a sharp transition in  $Nu(Ra)$ , from a low- $Ra$  regime with  $\gamma_{eff} = 0.308$  to an intermediate- $Ra$  range with  $\gamma_{eff} \simeq 0.25$ .<sup>‡</sup> At  $Ra^*$   $Nu$  is continuous and non-hysteretic, but  $\gamma_{eff}$  changes discontinuously. At somewhat larger  $Ra = Ra^{**} \simeq 3 \times 10^{14}$  a second transition takes place and a new state with  $\gamma_{eff} \simeq 0.17$  evolves. This second transition is followed by bistability of the  $\gamma_{eff} \simeq 0.25$  and the  $\gamma_{eff} \simeq 0.17$  state over the range  $3 \times 10^{14} \lesssim Ra \lesssim 8 \times 10^{14}$ .

Clearly the properties of the large- $Ra$  state that we found are quite different from the state envisioned by Kraichnan. Nonetheless, sharp transitions between two turbulent states, although known to occur under quite different circumstances [33], seem unlikely to occur unless they are provoked by changes in large-scale structures or boundary layers. For  $Ra < Ra^*$  it is well established that the Nusselt number is not sensitive to the nature of the LSC (see, for instance, Sect. III.F of [1]). Thus we presume that the changes in  $Nu(Ra)$  observed by us are caused by boundary-layer transitions. Of course much additional work should be done to investigate this issue in detail.

In the next section we briefly discuss some of the merits of compressed gases for the study of RBC at large  $Ra$ . We then give a detailed description of the experimental setup in Sect. 3. We discuss both the pressure vessel that we used (Sect. 3.1) and the high-pressure convection facility (Sect. 3.2) that was immersed in the pressure vessel. In Sect. 4 we show that the finite conductivity of the top and bottom plate had no significant influence on the measurements. Then, in Sect. 5, we present the results of

<sup>‡</sup> In our brief earlier publication[14] we reported the existence of the transition, but found an exponent above it that was somewhat larger than 0.25 albeit smaller than 0.308. This difference is due to the fact that we tried to correct for the finite conductivity of the top and bottom aluminum plates. We show below in Sect. 4 that such a correction is not appropriate for the present work with  $SF_6$  as the fluid. No such correction was applied to any of the data in this paper.

**Table 1.** Properties of various gases at a pressure of 19 bars, and of water and ethanol at 1 bar, all at 25°C.

fluid	$\lambda$ W/m K	$10^4\eta$ kg/s m	$10^6\lambda\eta$ W kg/s m <sup>2</sup> K	$10^{-8}\alpha/\kappa\nu$ s <sup>2</sup> /K m <sup>4</sup>	Pr
SF <sub>6</sub>	0.0154	0.1672	0.257	6846	0.86
N <sub>2</sub>	0.0266	0.1821	0.485	35.89	0.73
He	0.153	0.1977	3.018	0.526	0.67
H <sub>2</sub> O	0.606	8.9451	542	19.5	6.1
Ethanol	0.169	10.8247	183	97	15.6

the experiment. We conclude with a brief summary and discussion of the data.

## 2. Pure gases under pressure and large values of $Ra$

In Table 1 some relevant properties of SF<sub>6</sub>, N<sub>2</sub>, and He at a pressure of 19 bars (our maximum pressure) and a temperature of 25°C are compared with those of water and ethanol which are two typical liquids used in convection experiments.

The opportunities for achieving large  $Ra$  with compressed gases become apparent when we re-write Eq. 2 as

$$Ra = \frac{\alpha g \Delta T L^3 \rho^2 C_P}{\lambda \eta} \quad (5)$$

where  $\rho$  is the density,  $\eta = \rho\nu$  the shear viscosity, and  $\lambda = \rho C_P \kappa$  with  $C_P$  the heat capacity per unit mass. Noting that  $\eta$  and  $\lambda$  are only weakly dependent on  $P$ , one sees that  $Ra$  is proportional primarily to the square of the density. At constant  $\Delta T$  and for an ideal gas we then have

$$Ra \propto \rho^2 \propto P^2 M^2. \quad (6)$$

Here  $P$  is the pressure and  $M$  the molecular weight. To a good approximation this relation remains valid also for the real gases used in this work. Thus, high pressures and large  $M$  yield large  $Ra$ , and changing  $P$  and/or  $M$  will change the range of  $Ra$  accessible by varying  $\Delta T$ . Equation 6 motivated our choice of SF<sub>6</sub> with  $M = 146$  g/mole as the fluid for large- $Ra$  measurements. § Compared to liquids, gases also tend to have small values of  $\lambda$  and  $\eta$ . This can be seen from the examples given in Table 1. This is especially the case for gases with large  $M$  because, very roughly, the product of  $\lambda$  and  $\eta$  (see the table) is inversely proportional to the fourth power of the molecular diameter.[44] The

§ Sulfur hexafluoride was used before by Belmonte *et al.*[34, 35] to achieve values of  $Ra$  up to  $10^{11}$  for  $Pr = \mathcal{O}(1)$  in a much smaller apparatus with  $L \simeq 15$  cm. It was used also at pressures and temperatures near its critical point where  $Ra$  becomes exceptionally large, even for modest  $L$ ,[36] or where values of  $L$  as small as of order  $10\mu\text{m}$  can be used to study convection near onset[37, 38, 39, 41, 42, 43, 40]; but there  $Pr$  becomes large as well. All our work is in parameter ranges where  $Pr \simeq 0.8$  and where SF<sub>6</sub> behaves like a typical compressed gas .

small values of  $\eta\lambda$  further enhance the achievable values of  $Ra$ , especially for the heavier gases.

An additional advantage of using compressed classical gases is that the Prandtl number (see the table) will be nearly independent of  $P$  and close to the value  $2/3$  which is obtained from a simplified kinetic theory of a hard-sphere non-interacting gas.[44] For the measurements with cryogenic helium  $Pr$  increased as  $Ra$  became large (see, for instance, Fig. 2 of Ref. [14]) because the largest values of  $Ra$  were achieved by approaching the critical point where  $Pr$  diverges.

### 3. The apparatus

The apparatus consisted of a sample cell, known as the High Pressure Convection Facility of HPCF, inserted into a pressure vessel known as the “Uboot of Göttingen” and located at the Max Planck Institute for Dynamics and Self-Organization in Göttingen, Germany.

#### 3.1. The pressure vessel

The pressure vessel (see Fig. 1) consisted of a steel cylinder, with its axis positioned horizontally, of 5 m length and 2.5 m diameter. On the top side of the cylinder there was a turret of 1.5 m inner diameter and 1.5 m height; the resulting overall shape suggested the colloquial name “Uboot of Göttingen” for this facility. The upper part of the turret consisted of a bell-shaped dome that was removable. The HPCF was inserted into the turret with a crane capable of moving to any position in the experimental hall and of lifting up to 7000 kg. There were numerous feedthroughs entering the Uboot that could be used to bring electrical leads and water lines into or out of the interior. There also was a port of sufficient size to permit human access to the vessel interior. The vessel could be filled with various gases, including helium (He,  $Pr = 0.672$ ), nitrogen ( $N_2$ ,  $Pr = 0.723$  to  $0.729$ ), air ( $Pr = 0.707$ ), or sulfur hexa-fluoride ( $SF_6$ ,  $Pr = 0.79$  to  $0.86$ ). The maximum allowed pressure was 19 bars. The temperature of the Uboot could be adjusted over the range from 10 to 50°C. After use the  $N_2$ , air, or He was discharged outside the hall. There was a storage and recovery system for  $SF_6$ . The total volume of the Uboot was approximately 25 m<sup>3</sup> and required 3800 kg of  $SF_6$  for filling to maximum pressure.

#### 3.2. The High-Pressure Convection Facility (HPCF)

*3.2.1. The HPCF structure.* Two convection facilities were used. They had the same interior dimensions, with height  $L = 2.24$  m and diameter  $D = 1.12$  m, yielding aspect ratios  $\Gamma \equiv D/L = 0.500$ . The main difference between them was that one (HPCF-I) had aluminum top and bottom plates, whereas the other (HPCF-II) had copper plates. The aluminum was alloy 6082 with a thermal conductivity of 170 W/m K. The high-purity copper was of Deutsches Institut für Normung (DIN) type OF-Cu grade 1 (EN Cu-OFE-CW009A or ASTM C10100) with a conductivity of 394 W/m K.

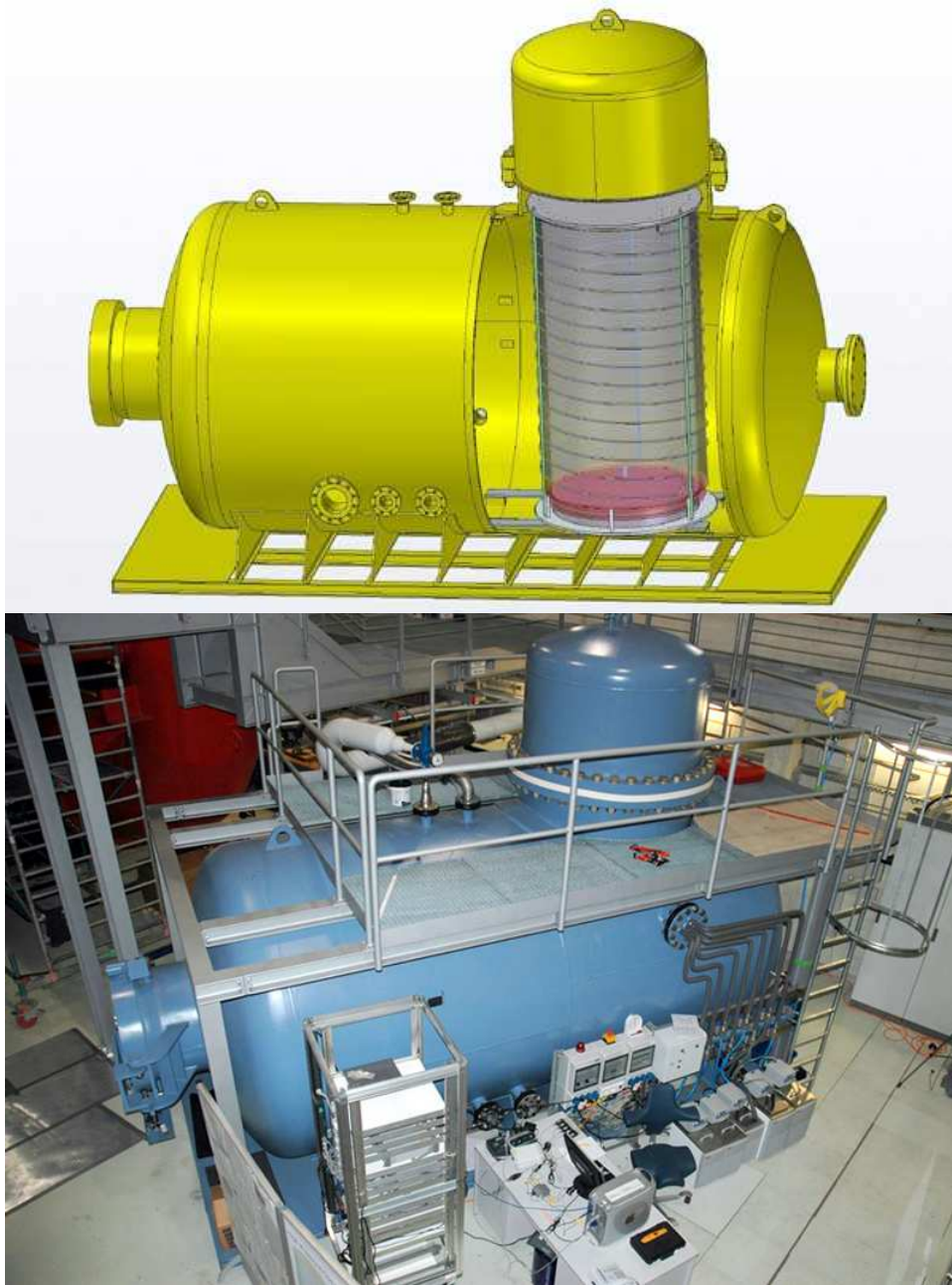


**Figure 1.** Top: A schematic diagram of the Uboot and the High Pressure Convection Facility (HPCF). Bottom: A photograph of the Uboot and associated instrumentation and services.

Figure 2 is a diagram (to scale) of the top and bottom right section, and Fig. 3 shows two photographs of the bottom section, of HPCF-II. We shall describe the facility starting at the bottom. A high-strength aluminum bottom support-plate (BSP) stood on three legs. The legs were of adjustable length to allow leveling of the bottom section of the facility. Supported on it by a steel bottom-shield support-ring (BSSR) of 4 mm thickness, 80 mm height, and 1120 mm diameter was a bottom shield (BS). The BS had two electrical resistance heaters. One, on its underside, was uniformly distributed over

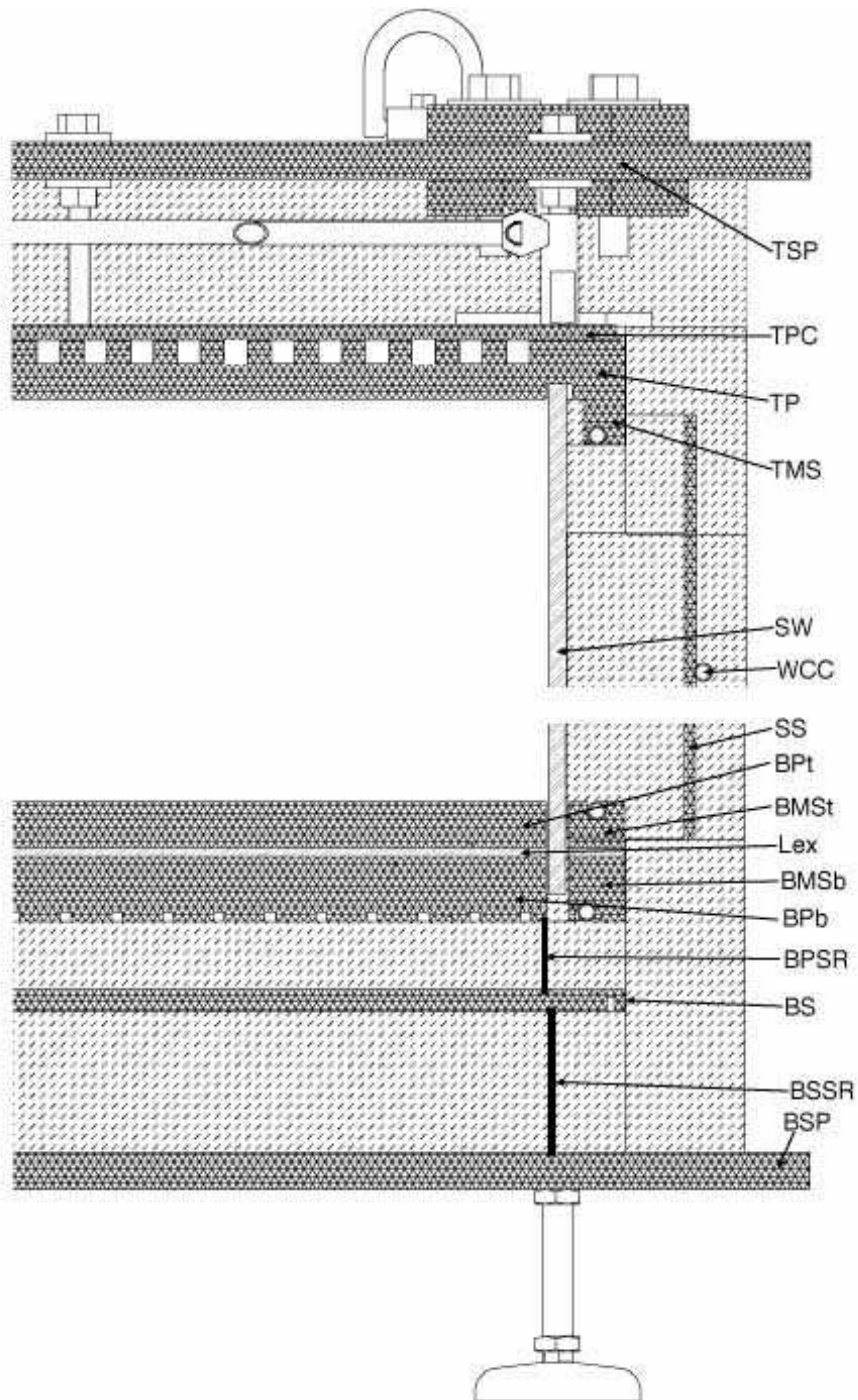


**Figure 2.** Schematic diagram of the HPCF-II (to scale). From bottom to top, we have the Bottom Support Plate BSP, the bottom shield support ring BSSR, the Bottom Shield BS, the bottom plate support ring BPSR, the Bottom Plate bottom BPb, the Lexan plate Lex, the Bottom Plate top BPt, the Bottom Microshield bottom BMSb, the Bottom Microshield top BMSt, the Side Shield SS with its water cooling coil WCC, the Plexiglas Side Wall SW, the Top Microshield TMS, the Top Plate TP, the Top Plate Cover TPC, and the Top Support Plate TSP.

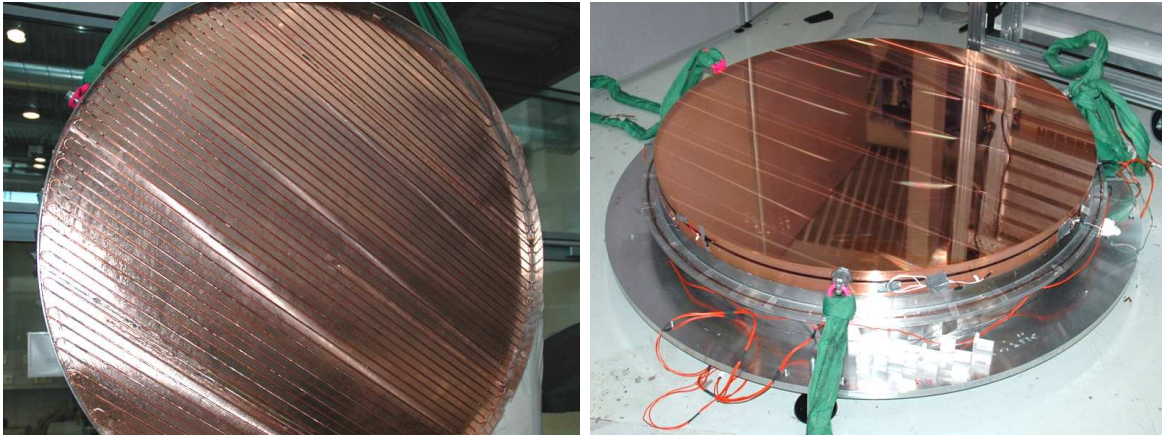


**Figure 3.** Left: The underside of the bottom-plate (BP) composite, showing the heater grooves in the BPb. The Bottom Plate Support Ring (BPSR) can be seen as well. Right: The entire bottom portion of HPCF-II, showing (from bottom to top) the Bottom Support Plate (BSP), the Bottom Shield (BS), the Bottom-Plate Support ring (BPSR), and the bottom-plate composite with the Lexan sheet between the BPb and the BPt. The mirror finish of the BPt is apparent.

the area inside of the BSSR. The other was in a circular groove extending around the circumference just outside of the BSSR. Two thermometers were located on the top side of the BS, one (TBS) near its center and the other (TBSaux) near the BSSR. At both locations the temperature was regulated, using the two heaters, at the temperature of the bottom plate above it.

A composite bottom plate was supported on a steel support ring (BPSR) of 4mm thickness, 40 mm height, and 1120 mm diameter. It consisted of a 35 mm thick bottom (BPb) and a 25 mm thick top (BPt) plate (aluminum for HPCF-I and copper for HPCF-II) with a Lexan (Lex) plate of 5 mm thickness between them. These three plates were glued together using degassed Stycast 1266 epoxy, with care being taken to avoid the trapping of air bubbles. We estimate that each epoxy film had a thickness of less than 0.1 mm. The top surface of the BPt (see Fig. 3 right), which faced the fluid, was machined to a mirror finish. For the copper plates the mean roughness  $R_a$ , measured with a Mahr perthometer at several locations, was typically about  $0.2 \mu\text{m}$ . For the aluminum plates  $R_a$  was around  $1.6 \mu\text{m}$ .

The Plexiglas side wall (SW) with an inner diameter of 1.12 m and a wall thickness of 9 mm extended downward over all of the BPt, the Lexan plate, and part of the BPb. The BPb and BPt were each surrounded by a thermal “micro-shield” (BMSb and BMSt) made of aluminum. The temperature of BMSb was regulated at the temperature of the BPb by temperature controlled water circulating through a coil imbedded in the aluminum. The BMSt was similarly regulated at the temperature of the BPt. The side wall was surrounded by an aluminum side shield (SS) of 2.23 m length, 1.26 m inner diameter, and 6 mm wall thickness. The SS temperature was regulated by temperature controlled water circulating through copper coils (WCC) wrapped around and attached

to its outside; the WCC consisted of two anti-parallel water circuits and covered the entire length of the SS with many turns with a spacing of 76 mm between them.

Focusing now on the very top of the HPCF, there was a high-strength aluminum top support plate (TSP), which was supported from the BSP by three aluminum support structures (not shown in the figure) spaced azimuthally at  $120^\circ$ . Hanging from the TSP was the top plate assembly. For HPCF-II it consisted of the copper top plate (TP) of 35 mm thickness containing cooling-water channels and a copper top-plate cover (TPC) of 5 mm thickness which was sealed to the TP by Stycast 1266 epoxy and numerous screws around the circumference. For HPCF-I the top plate was similar, but made of aluminum. The TP could be leveled using threaded posts and nuts that terminated the top of the support structures. Care was taken to make sure that the TP did not rest on the SW, but the SW extended several mm into a groove in the TP. The bottom surface of the TP, which faced the fluid, was machined to a mirror finish similar to that of the BPt.

An important issue was the insulation that could be provided outside of the actual cell. For HPCF-I the entire lightly shaded area shown in Fig. 2 was filled with low-density open-pore foam. Although this provided adequate insulation for the measurements with helium [32], nitrogen, and  $\text{SF}_6$  at modest  $Ra$ , it became apparent that convection outside the cell and in the foam was occurring during measurements at the highest  $Ra$ . This convection could lead to erroneous determinations of the heat transport inside the cell. It limited the work with HPCF-I to  $Ra \lesssim 3 \times 10^{14}$ , as will be apparent from the data displayed below in Figs. 6 and 7.

For HPCF-II two versions were used with different levels of insulation in addition to that of HPCF-I. In the first, HPCF-IIa, we used several alternating layers of 4 mm thick open-pore foam and thin polyester film in critical locations where large thermal gradients were expected to occur. The film was intended to prevent any large-scale flow in critical regions outside the cell. Particularly important was the area immediately outside of the BMSb and the BMSt as well as outside the TMS and the TP. These layers extended a small distance down or up over the side wall. Finally, for HPCF-IIb we added three layers of 4 mm foam and film over the entire length of the SW, and blocked off almost completely the entrance to the space between the SS and the SW at the top and bottom adjacent to the TMS and the BMSt by film so as to avoid gas circulation through the entire system. Insofar as all three versions of the HPCF yielded equivalent results for  $Nu(Ra)$ , we feel confident that the measurements truly pertain to properties of the cylindrical convection cell.

The total weight of HPCF-II was about 2000 kg. The facility was assembled outside the Uboot and lifted with a crane using three ropes attached to eyes screwed into the BSP. With the Uboot dome removed, the HPCF was inserted into the turret of the Uboot (see Fig. 4 of Ref. [2]). The dome was then replaced. After all electrical and water connections were made, the Uboot was closed and evacuated to a residual pressure of 1 mTorr. When He or  $\text{N}_2$  were used, the system was pressurized to 0.5 bars and re-evacuated (with  $\text{SF}_6$  this flushing procedure was not feasible). The Uboot was then

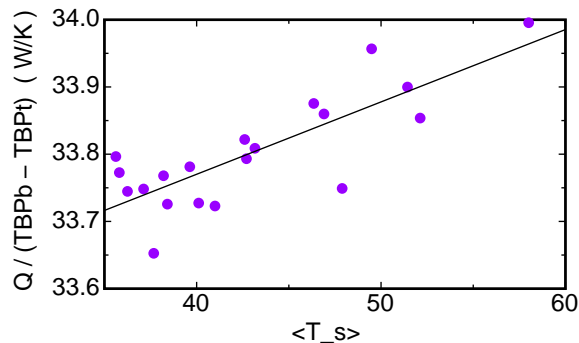


**Figure 4.** The conductance  $Q/(TBPb - TBPt)$  of the bottom-plate composite for HPCF-I, determined with nitrogen as the fluid and for  $Ra \lesssim 3 \times 10^{12}$ .

pressurized in steps of 0.5 bars every five minutes up to the desired pressure.

*3.2.2. Heating and cooling of the plates.* The underside of the BPb was covered uniformly by grooves of 50 m total length, spaced 19 mm apart and connected at their ends, 4 mm wide, and 5 mm deep (see Fig. 3 left). American Wire Gage (AWG) 24 copper magnet wire was epoxied into the grooves and provided a heater with a resistance of about  $4.1 \Omega$ . Care was taken to position the wire close to the bottom of the groove, imbedded in the epoxy. The heater was driven by an Agilent model 6675A power supply and could deliver up to 1.3 kW. From the wire resistance we inferred that it warmed up to about  $75^\circ\text{C}$  at a current of 18 Amp when the plate was at  $25^\circ\text{C}$ . The power dissipated was determined from the current supplied by the power supply and the measured voltage across the heater.

The actual heat input to the sample fluid was determined from the temperature difference between the two copper plates of the bottom-plate assembly. The conductance of the assembly was determined using the heat input to the bottom-plate heater under conditions where all the Joule heat passed into the sample. This situation prevailed when the Rayleigh number was not too large and convection outside the cell was virtually absent. These conditions were satisfied primarily during the measurements with helium and nitrogen. The calibration data for HPCF-I are shown in Fig. 4. We found

$$Q = 33.3(1 + 3.2 \times 10^{-4} \langle T_S \rangle)(TBPb - TBPt) \quad (7)$$

where  $Q$  is in Watts,  $\langle T_S \rangle = (TBPb + TBPt)/2$  in  $^\circ\text{C}$ , and  $TBPb$  and  $TBPt$  are the temperatures of BPb and BPt respectively. As can be seen, this calibration depended weakly upon the mean temperature  $\langle T_S \rangle$  of the composite because the conductivity of Lexan is temperature dependent. At a given  $\langle T_S \rangle$  it was independent of  $TBPb - TBPt$  or the applied heat current since the conduction in the composite is a linear process.

The top plate was cooled by water passing through quadruple spiral grooves of 12.7 mm width and 12.6 mm depth that had been machined into the top plate. The spacing between adjacent grooves was 25 mm. The spirals were inter-connected so that

they created two parallel circuits, with each of them spiraling inward and then outward again. Cooling or heating was provided by a Neslab RTE-740 temperature controlled circulator with a cooling capacity of 800 W. When greater cooling power was needed, a second such circulator was used to pass its water through cooling coils immersed in the reservoir of the first.

*3.2.3. Thermometry.* The system contained 26 thermistors that had been calibrated in a separate calibration facility with a precision of a mK against a Hart Scientific Model 5626 platinum resistance thermometer which in turn had been calibrated against various fixed points on the ITS-90 temperature scale by the Hart Scientific Division of Fluke Corporation. As mentioned, TBS and TBSaux were located on the bottom shield. The BPb, BPt, and TP each had five thermometers inserted into them in small-diameter holes that extended within 3 mm of a plate surface. In each case one thermometer (TBPb0, TBPt0, TTP0) was located at the plate center. Four more (TBP1 to TBP4 etc.) were uniformly spaced in the azimuthal direction on a circle of 950 mm diameter. The thermometers in BPb and BPT were located near the top surface of the plate, while those in the TP were located near the bottom surface close to the fluid.

Two thermometers (TBMSb0 and TBMSb1 etc.) were located in each of the micro-shields, azimuthally spaced at  $180^\circ$ .

Three thermometers were located inside the side shield. One was at half height and the other two at a distance of 60 mm from the top or bottom.

In addition, there were 24 uncalibrated smaller thermistors located in small blind holes drilled into the side wall. Eight were at locations spaced uniformly in the azimuthal direction at the horizontal mid-plane ( $z = 0$ ), and eight each were similarly positioned at the vertical positions  $z = \pm L/4$ .

#### 4. Top- and bottom-plate correction

For modest values of  $Ra$ , in the range  $Ra < Ra^*$ , it was understood some time ago on the basis of DNS that the finite conductivity of the top and bottom plate of the convection cell may reduce  $Nu$  below its ideal value for constant-temperature boundary conditions.[45] Experimentally this effect was confirmed for  $Ra \lesssim 10^{12}$  using water as the fluid and pairs of nominally identical sample cells,[46], one of each pair with aluminum plates with a plate conductivity  $\lambda_p = 170\text{W/m K}$  and the other with copper plates with  $\lambda_p = 400\text{W/m K}$ . The copper plates yielded larger values for  $Nu$ . This result was part of the motivation for building both HPCF-I with aluminum plates and HPCF-II with copper plates. It was noted before[32] that the plate correction is unimportant for measurements with helium gas for  $Ra \lesssim 10^{11}$ , but for  $\text{SF}_6$  and  $Ra = \mathcal{O}(10^{14})$  or more one would expect it to be larger and thus this case had to be re-examined.

In Fig. 5 we show data from HPCF-I as circles and those from HPCF-II as squares. The solid symbols are the measured values, without any attempt at a correction for the finite plate conductivity. One sees that the copper-plate data fall *below* the aluminum-

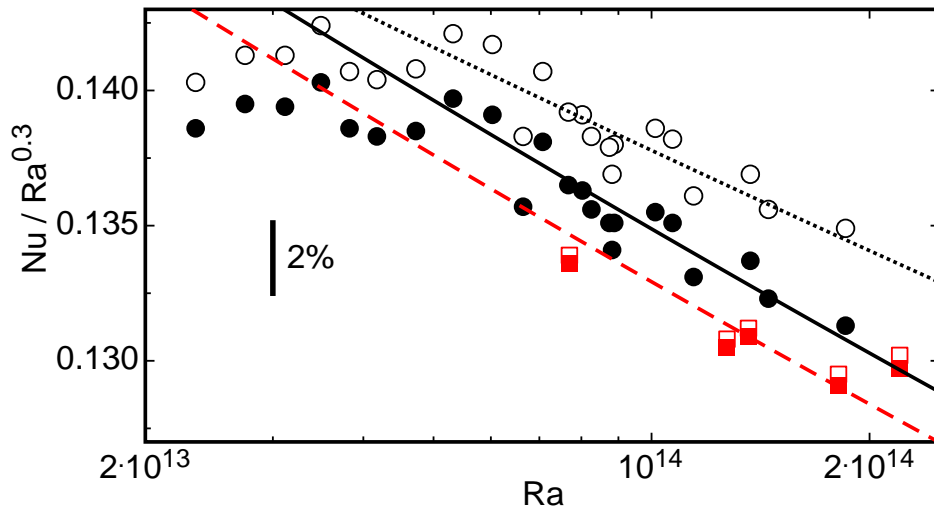


**Figure 5.** The reduced Nusselt number  $Nu/Ra^{0.3}$  as a function of the Rayleigh number  $Ra$  on a logarithmic scale. Circles: from HPCF-I with aluminum top and bottom plates. Squares: from HPCF-II with copper plates. Solid symbols: as measured. Open symbols: after a correction for the finite conductivity of the plates as described in the text. The lines are fits to the data. Clearly the correction causes a greater disagreement between the two data sets and should not be applied to these measurements.

plate data, whereas a finite conductivity effect would have produced the opposite result. The two data sets, within their experimental scatter, can be represented by parallel lines (solid and dashed) separated by about 1.5%. This difference is within possible systematic errors arising from the calibrations of the thermal resistances of the bottom-plate composites and other sources. Thus we conclude that within our resolution the data are not influenced by the finite plate conductivity and correspond within experimental uncertainties to the ideal case.

Although the plate effect seems unimportant for the present measurements with  $SF_6$ , it is of interest to see how large it is predicted to be using the information obtained with water as the fluid. The water measurements could be described well by a correction factor  $f(X)$ , with

$$Nu = f(X)Nu_{\infty} . \quad (8)$$

where  $Nu_{\infty}$  is the ideal Nusselt number in the presence of perfectly conducting rigid top and bottom plates. The argument  $X$  is the ratio of the thermal resistance of the fluid to that of an end plate, i. e.

$$X = R_f/R_p \quad (9)$$

$$= X_0/Nu ; \quad (10)$$

$$X_0 \equiv \lambda_p L/(\lambda_f e) \quad (11)$$

with  $R_f$  and  $R_p$  equal to the resistances of the fluid and of a plate respectively. Here  $\lambda_p$  and  $\lambda_f$  are the end-plate and fluid conductivities respectively, and  $e$  is the thickness of

one plate. The data showed that the form

$$f(X) = 1 - \exp[-(aX)^b] . \quad (12)$$

provided a good description of the reduction. A simultaneous fit of the data with copper and with aluminum plates to

$$Nu = N_0 Ra^{\gamma_{eff}} f(X) , \quad (13)$$

yielded the parameters  $a$  and  $b$  (for more detail see [46]).

It turned out that within experimental resolution  $a$  and  $b$  were independent of  $\Gamma$  but dependent on the sample diameter  $D$ . An extrapolation (of considerable uncertainty) of  $a$  and  $b$  to  $D = 1$  m yielded  $a = 0.25$  and  $b = 0.32$ . [1] A correction with these parameters was applied to the data from HPCF-I that were published before. [14] Values of  $Nu_\infty$  computed with these values are shown in Fig. 5 as open symbols. This correction had very little effect upon the HPCF-II (copper plate) data but increased the HPCF-I data considerably. It caused the best-fit lines through them (dashed and dotted) to be non-parallel. Clearly this correction is inappropriate for the SF<sub>6</sub> data. It seems likely to us that the model for the plate correction used before [45] is incomplete. It comes to mind that the correction may depend as well upon the heat capacity per unit volume, which is about a factor of 30 smaller for SF<sub>6</sub> at 19 bars than it is for water.

## 5. Results

In Fig. 6 we show our measurements of  $Nu$  as a function of  $Ra$  on logarithmic scales. Also shown are the results of Chavanne *et al.* [28] (plusses) and those of Niemela *et al.* (stars). For  $Ra \lesssim 4 \times 10^{13}$  our results could be fit well by Eq. 4 with  $N_0 = 0.112$  and  $\gamma_{eff} = 0.308$ , as shown by the dashed line in the figure. The data are reasonably consistent with those of Niemela *et al.* [30, 31], although the effective exponent derived from them is a little smaller than their  $\gamma_{eff} = 0.32$  [31]. As discussed before, [14] our data do not show the transition near  $Ra = 10^{11}$  to a power-law dependence with an exponent of about 0.4 that was reported in Refs. [27, 28] and interpreted there as the transition to the ultimate state discussed by Kraichnan [13].

In Fig. 6 it can be seen that our measurements fall increasingly below the dashed line as  $Ra$  increases beyond about  $4 \times 10^{13}$ . In order to see this phenomenon more clearly, we show in Fig. 7 the reduced Nusselt number  $Nu/Ra^{0.3}$ , which for  $\gamma_{eff} = 0.308$  is nearly constant and thus can be displayed with much greater resolution. There we see a well defined transition in  $Nu(Ra)$  at  $Ra^* \simeq 4 \times 10^{13}$ . At  $Ra^*$   $Nu$  is continuous, but  $\gamma_{eff}$  changes discontinuously from 0.308 to a lesser value. A fit of Eq. 4 to data with  $Ra > Ra^*$  yielded  $N_0 = 0.603$  and  $\gamma_{eff} = 0.253$ ; this fit is shown as the solid red line in the figure.

Further examination of Fig. 7 shows that there is an additional surprise. For  $Ra \gtrsim Ra^{**} \simeq 2 \times 10^{14}$  the system exhibits bistability. There is a large-Nusselt, or upper, branch of  $Nu(Ra)$  which is indistinguishable within our resolution from the one that formed at  $Ra^*$ . However, there also is a lower branch which corresponds to

nus\_keep\_He.data

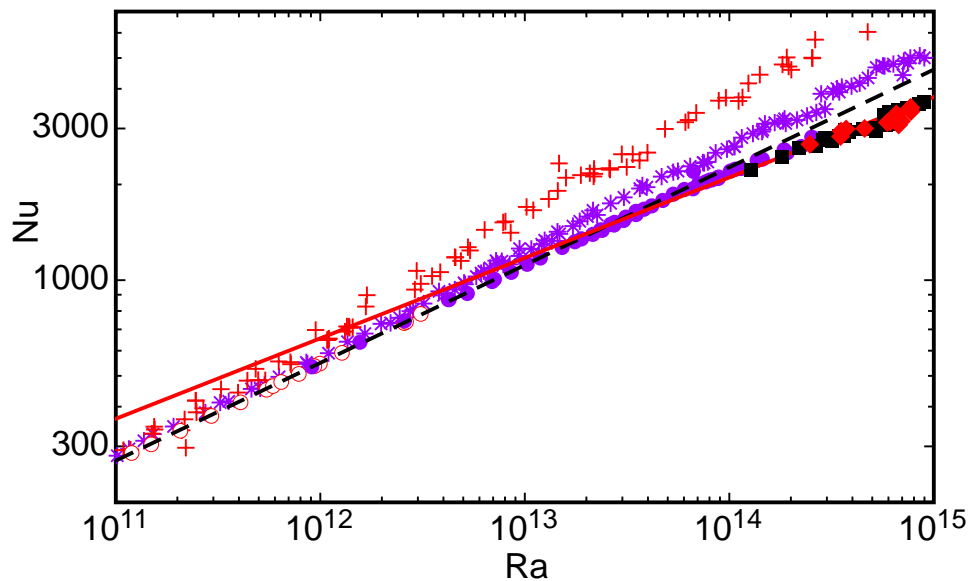


**Figure 6.** The Nusselt number  $Nu$  as a function of the Rayleigh number  $Ra$  on logarithmic scales. Open circles:  $N_2$ . Solid symbols:  $SF_6$ . Purple circles: HPCF-I. Black squares: HPCF-IIa. Red diamonds: HPCF-IIb. Black dashed line: power-law fit to the data for  $Ra \lesssim 10^{13}$ . This line corresponds to an exponent  $\gamma_{eff} = 0.308$ . Red solid line: a power-law fit to the data on the upper branch for  $Ra \gtrsim 5 \times 10^{13}$ . This line corresponds to an exponent  $\gamma_{eff} = 0.25$ . For comparison we show the data of Niemela *et al.* [31] as purple stars and those of Chavanne *et al.* [28] as red plusses.

$N_0 = 9.5$  and  $\gamma_{eff} = 0.17$ . A powerlaw with those parameters is shown in Fig. 7 by the purple dotted line. The data indicate that the transition to a final state is a complex phenomenon involving at least two steps with the second one involving bi-stability.

The unexpected nature of the phenomena revealed by our data motivated us to make the various modifications in the HPCF that were discussed in the experimental section. As can be seen from the figure, the data obtained with HPCF-I (open red and solid purple circles), HPCF-IIa (black solid squares), and HPCF-IIb (red solid diamonds) are all consistent with each other wherever they overlap. Thus we feel confident at this point that the observed branches of  $Nu(Ra)$  are genuine properties of convection in the cylindrical sample with  $\Gamma = 0.50$  rather than some artifact of the experiment.

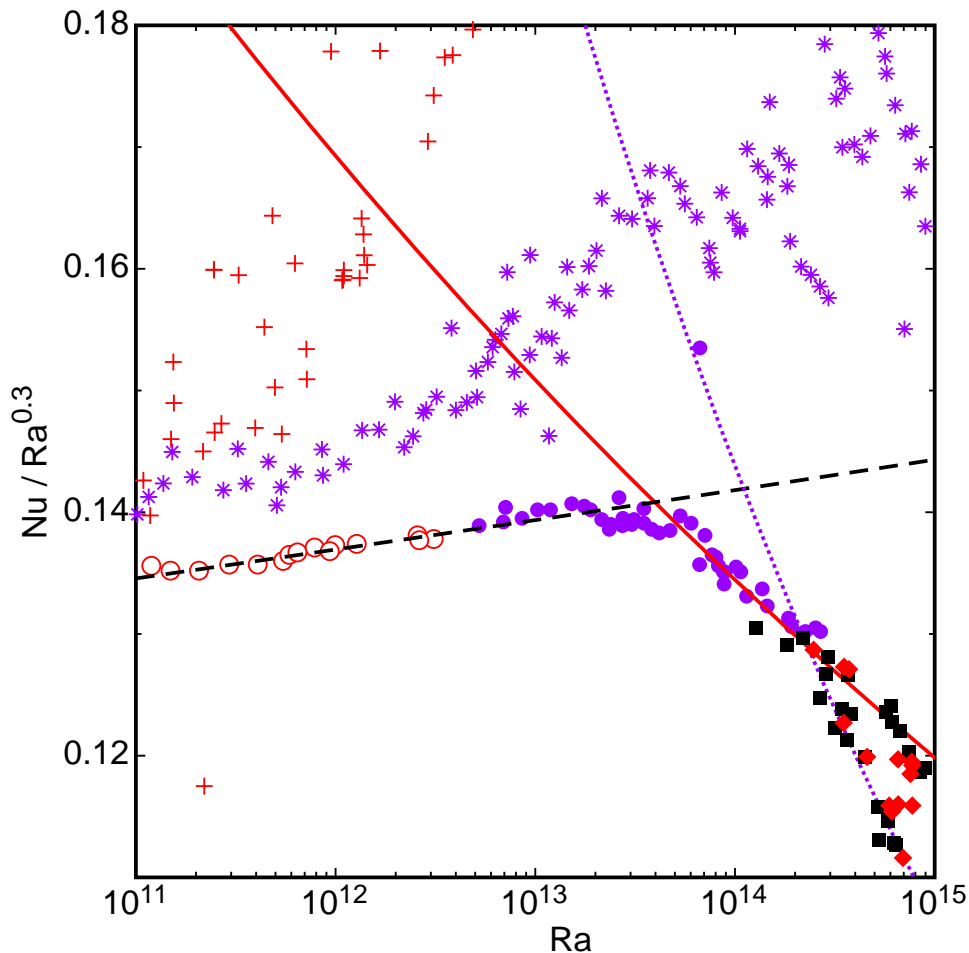


**Figure 7.** The reduced Nusselt number  $Nu/Ra^{0.3}$  as a function of the Rayleigh number  $Ra$  on a logarithmic scale. The symbols, dashed line, and solid line are as in Fig. 6. The purple dotted line corresponds to  $\gamma_{eff} = 0.17$ .

## 6. Summary and discussion

In this paper we described a new facility for the study of turbulent Rayleigh-Bénard convection in gases under pressures of up to 19 bars and presented results for the turbulent heat transport, as expressed by the Nusselt number  $Nu$  (see Eq. 1) for a cylindrical sample of aspect ratio  $\Gamma = 0.500$ . We used nitrogen and sulfur hexa-fluoride as the fluids. We found that the dependence of  $Nu$  upon the Rayleigh number  $Ra$  can be described well by a power law with an effective exponent  $\gamma_{eff} = 0.308$  when  $Ra < Ra^* \simeq 4 \times 10^{13}$ . At  $Ra^*$  there was a transition to a new state. At the transition  $Nu$  was continuous, but  $\gamma_{eff}$  changed suddenly to a value close to 0.25. At somewhat larger  $Ra = Ra^{**} \simeq 3 \times 10^{14}$  there was a further change of  $Nu(Ra)$ . A new branch characterized by  $\gamma_{eff} \simeq 0.17$  arose and co-existed with the  $\gamma_{eff} = 0.25$  branch.

The continuity of  $Nu$  and the sharpness of the transition at  $Ra^*$  suggest the existence of a supercritical bifurcation from one turbulent state to another. A similar phenomenon was observed recently in turbulent RBC in the presence of rotation.[33] In

that case the bifurcation is believed to be due to the formation of a new macroscopic structure in the turbulent flow, namely due to the formation of Ekman vortices. Indeed it is hard to imagine a bifurcation connecting two turbulent states unless it is accompanied by changes in the large scales or in the boundary conditions. For RBC without rotation the dominant large scale is a single convection roll known as the large-scale circulation or LSC. It has been established quite well by experiment that changes of the LSC do not influence the Nusselt number significantly (see, for instance, Sect. III.F of [1]). Thus we expect in the present case that the transition is caused by a change in the nature of the viscous and thermal boundary layers. As discussed in the Introduction, such a change is expected at the transition to the ultimate state, and the value of  $Ra^*$  is only a little smaller than the estimate by Grossmann and Lohse [20] for the stability limit of the laminar viscous boundary layer in the presence of the shear applied by the LSC. However, the state that we find above the transition clearly is very different from the one envisioned by Kraichnan [13] which would have  $\gamma_{eff} \simeq 0.4$  rather than 0.25 or 0.17.

Since we can only speculate about the cause of the transition at  $Ra^*$ , we really are not in any position to even guess at the cause of the second transition at  $Ra^{**}$  to the bistable range of  $Ra$ .

An obvious question that arises is whether the transitions found by us should have been revealed by the data of Niemela *et al.* [30, 31] which are shown as purple stars in Fig. 7. One might argue that those data do show a change in  $Nu(Ra)$  near  $Ra = 4 \times 10^{13}$ , but really the scatter is too large to be sure. In this connection it is noteworthy that for the data of Ref. [31] the Prandtl number increased with  $Ra$ ; at  $Ra = 4 \times 10^{13}$  it had grown to about 1.0 and it increased fairly rapidly for larger  $Ra$ . We can not say whether this prevented the observation of the bifurcations that we observed.

## Acknowledgments

We are very grateful to the Max-Planck-Society and the Volkswagen Stiftung, whose generous support made the establishment of the facility and the experiments possible. The work of G.A. was supported in part by the U.S National Science Foundation through Grant DMR07-02111. We are very grateful to Artur Kubitzek and Andreas Renner for their enthusiastic technical support and to Holger Nobach for his role in developing the SF<sub>6</sub> system.

- [1] G. Ahlers, S. Grossmann, and D. Lohse, *Heat transfer and large scale dynamics in turbulent Rayleigh-Bénard convection*, Rev. Mod. Phys. **81**, 503 (2009).
- [2] G. Ahlers, *Turbulent convection*, Physics **2**, 74 (2009).
- [3] D. Lohse and K.-Q. Xia, *Small-scale properties of turbulent Rayleigh-Bénard convection*, Annu. Rev. Fluid Mech. **42**, 335 (2010).
- [4] P. Cardin and P. Olson, *Chaotic thermal convection in a rapidly rotating spherical shell: consequences for flow in the outer core*, Phys. of the Earth and Planetary Interiors **82**, 235 (1994).
- [5] G. Glatzmaier, R. Coe, L. Hongre, and P. Roberts, *The role of the Earth's mantle in controlling the frequency of geomagnetic reversals*, Nature(London) **401**, 885 (1999).

- [6] E. van Doorn, B. Dhruva, K. R. Sreenivasan, and V. Cassella, *Statistics of wind direction and its increments*, Phys. Fluids **12**, 1529 (2000).
- [7] D. L. Hartmann, L. A. Moy, and Q. Fu, *Tropical convection and the energy balance at the top of the atmosphere*, J. Climate **14**, 4495 (2001).
- [8] J. Marshall and F. Schott, *Open-ocean convection: Observations, theory, and models*, Rev. Geophys. **37**, 1 (1999).
- [9] S. Rahmstorf, *The thermohaline ocean circulation: A system with dangerous thresholds?*, Climate Change **46**, 247 (2000).
- [10] F. Cattaneo, T. Emonet, and N. Weiss, *On the interaction between convection and magnetic fields*, Astrophys. J. **588**, 1183 (2003).
- [11] F. H. Busse, Chaos **4**, 123 (1994).
- [12] S. Grossmann and D. Lohse, *Thermal convection for large Prandtl number*, Phys. Rev. Lett. **86**, 3316 (2001).
- [13] R. H. Kraichnan, *Turbulent thermal convection at arbitrary Prandtl number*, Phys. Fluids **5**, 1374 (1962).
- [14] D. Funfschilling, E. Bodenschatz, and G. Ahlers, *Search for the “ultimate state” in turbulent Rayleigh-Bénard convection*, Phys. Rev. Lett. **103**, 024503 (2009).
- [15] E. Brown and G. Ahlers, *Effect of the Earth’s Coriolis force on turbulent Rayleigh-Bénard convection in the laboratory*, Phys. Fluids **18**, 125108 (2006).
- [16] E. Brown and G. Ahlers, *Large-scale circulation model of turbulent Rayleigh-Bénard convection*, Phys. Rev. Lett. **98**, 134501 (2007).
- [17] E. Brown and G. Ahlers, *A model of diffusion in a potential well for the dynamics of the large-scale circulation in turbulent Rayleigh-Bénard convection*, Phys. Fluids **20**, 075101 (2008).
- [18] E. Brown and G. Ahlers, *Azimuthal asymmetries of the large-scale circulation in turbulent Rayleigh-Bénard convection*, Phys. Fluids **20**, 105105 (2008).
- [19] L. D. Landau and E. M. Lifshitz, *Fluid Mechanics* (Pergamon Press, Oxford, 1987).
- [20] S. Grossmann and D. Lohse, *Prandtl and Rayleigh number dependence of the Reynolds number in turbulent thermal convection*, Phys. Rev. E **66**, 016305 (2002).
- [21] K. R. Sreenivasan and R. J. Donnelly, *Role of cryogenic helium in classical fluid dynamics: Basic research and model testing*, Adv. Appl. Mech. **37**, 239 (2001).
- [22] G. Ahlers, *Low-temperature studies of the Rayleigh-Bénard instability and turbulence*, Phys. Rev. Lett. **33**, 1185 (1974).
- [23] D. C. Threlfall, *Free convection in low temperature gaseous helium*, J. Fluid Mech. **67**, 17 (1975).
- [24] G. Ahlers, in *Fluctuations, Instabilities and Phase Transitions*, edited by T. Riste (Plenum, New York, 1975), pp. 181–193.
- [25] B. Castaing, G. Gunaratne, F. Heslot, L. Kadanoff, A. Libchaber, S. Thomae, X. Z. Wu, S. Zaleski, and G. Zanetti, *Scaling of hard thermal turbulence in Rayleigh-Bénard convection*, J. Fluid Mech. **204**, 1 (1989).
- [26] X. Chavanne, F. Chillá, B. Chabaud, B. Castaing, J. Chauussy, and B. Hébral, *High Rayleigh number convection with gaseous helium at low temperature*, J. Low Temp. Phys. **104**, 109 (1996).
- [27] X. Chavanne, F. Chilla, B. Castaing, B. Hébral, B. Chabaud, and J. Chauussy, *Observation of the ultimate regime in Rayleigh-Bénard convection*, Phys. Rev. Lett. **79**, 3648 (1997).
- [28] X. Chavanne, F. Chilla, B. Chabaud, B. Castaing, and B. Hébral, *Turbulent Rayleigh-Bénard convection in gaseous and liquid He*, Phys. Fluids **13**, 1300 (2001).
- [29] R. J. Donnelly, in *Flow at ultra-high Reynolds and Rayleigh numbers, a status report*, edited by R. J. Donnelly and K. R. Sreenivasan (Springer, New York, 1984), pp. 1 – 28.
- [30] J. J. Niemela, L. Skrbek, K. R. Sreenivasan, and R. Donnelly, *Turbulent convection at very high Rayleigh numbers*, Nature **404**, 837 (2000).
- [31] J. J. Niemela and K. R. Sreenivasan, *The use of cryogenic helium for classical turbulence: Promises and hurdles*, J. Low Temp. Phys. **143**, 163 (2006).
- [32] G. Ahlers, E. Bodenschatz, D. Funfschilling, and J. Hogg, *Turbulent Rayleigh-Bénard convection*

- for a Prandtl number of 0.67, *J. Fluid Mech.* **in press**, ?? (2009).
- [33] R. Stevens, J.-Q. Zhong, H. Clercx, G. Ahlers, and D. Lohse, *Transitions between turbulent states in rotating Rayleigh-Bénard convection*, *Phys. Rev. Lett.* **103**, 024503 (2009).
- [34] A. Belmonte, A. Tilgner, and A. Libchaber, *Boundary layer length scales in thermal turbulence*, *Phys. Rev. Lett.* **70**, 4067 (1993).
- [35] A. Belmonte, A. Tilgner, and A. Libchaber, *Temperature and velocity boundary layers in turbulent convection*, *Phys. Rev. E* **50**, 269 (1994).
- [36] S. Ashkenazi and V. Steinberg, *High Rayleigh number turbulent convection in a gas near the gas-liquid critical point*, *Phys. Rev. Lett.* **83**, 3641 (1999).
- [37] M. Assenheimer and V. Steinberg, *Rayleigh-Bénard convection near the gas-liquid critical point*, *Phys. Rev. Lett.* **70**, 3888 (1993).
- [38] M. Assenheimer and V. Steinberg, *Transition between spirals and target states in Rayleigh-Bénard convection*, *Nature* **367**, 345 (1994).
- [39] K. M. S. Bajaj, N. Mukolobwicz, N. Currier, and G. Ahlers, *Wavenumber selection and large-scale-flow effects due to a radial ramp of the spacing in Rayleigh-Bénard convection*, *Phys. Rev. Lett.* **83**, 5282 (1999).
- [40] K. M. S. Bajaj, N. Mukolobwicz, J. Oh, and A. G., *Rayleigh-Bénard convection in the presence of a radial ramp of the Rayleigh number*, *J. Stat. Mech.* **P02001**, P02001 (2006).
- [41] A. Roy and V. Steinberg, *Reentrant hexagons in non-Boussinesq Rayleigh-Bénard convection: Effect of compressibility*, *Phys. Rev. Lett.* **88**, 244503 (2002).
- [42] J. Oh and G. Ahlers, *Thermal-Noise effect on the transition to Rayleigh-Bénard convection*, *Phys. Rev. Lett.* **91**, 094501 (2003).
- [43] J. Oh, J. M. Ortiz de Zárate, J. V. Sengers, and G. Ahlers, *Dynamics of fluctuations in a fluid below the onset of Rayleigh-Bénard convection*, *Phys. Rev. E* **69**, 021106 (2004).
- [44] J. O. Hirschfelder, C. F. Curtiss, and R. B. Bird, *Molecular Theory of Gases and Liquids* (John Wiley & Sons, New York, 1964).
- [45] R. Verzicco, *Effect of non-perfect thermal sources in turbulent thermal convection*, *Phys. Fluids* **16**, 1965 (2004).
- [46] E. Brown, A. Nikolaenko, D. Funfschilling, and G. Ahlers, *Heat transport by turbulent Rayleigh-Bénard convection: Effect of finite top- and bottom-plate conductivity*, *Phys. Fluids* **17**, 075108 (2005).